HtrA, fatty acids, and membrane protein interplay in Chlamydia trachomatis to impact stress response and trigger early cellular exit

HtrA, fatty acids, and membrane proteins interplay in *Chlamydia trachomatis* to impact stress response and trigger early cellular exit

Fatty acids, HtrA, and stress response in *Chlamydia*

Natalie Strange[1*], Laurence Luu[1*], Vanissa Ong[2], Bryan A. Wee[2,3], Matthew J. A. Phillips[1], Laura McCaughey[4,5], Joel R. Steele[1,6], Christopher K. Barlow[6], Charles G. Cranfield[1], Garry Myers[4], Rami Mazraani[1], Charles Rock[7], Peter Timms[8], Wilhelmina M. Huston[9#]

[1] School of Life Sciences, Faculty of Science, University of Technology Sydney, 15 Broadway, Ultimo, NSW 2007, Australia

[2] Faculty of Health, Queensland University of Technology Kelvin Grove, QLD 4059, Australia

[3] The Roslin Institute, University of Edinburgh, Midlothian, EH25 9RG, Scotland, United Kingdom

[4] Australian Institute for Microbiology and Infection, Faculty of Science, University of Technology Sydney, 15 Broadway, Ultimo, NSW 2007, Australia

[5] School of Infection and Immunity, College of Medical, Veterinary and Life Sciences, University of Glasgow, G12 8QQ, Scotland

[6] Monash Proteomics and Metabolomics Platform, Department of Biochemistry and Molecular Biology, Monash Biomedicine Discovery Institute, Monash University, Clayton, VIC 3168, Australia

23 [7] Department of Infectious Diseases, St. Jude Children's Research Hospital, Memphis,
24 Tennessee, 38015, USA

25 [8] Centre for Bioinnovation, University of the Sunshine Coast, Maroochydore, QLD 4558,
26 Australia

27 [9] Faculty of Science, University of Technology Sydney, 15 Broadway, Ultimo, NSW 2007,
28 Australia

29

30 * these authors contributed equally to the work

31 [#]Correspondent footnote: Wilhelmina.Huston@uts.edu.au

32

33

Abstract *Chlamydia trachomatis* is an intracellular bacterial pathogen that undergoes a bi-phasic developmental cycle, consisting of intracellular reticulate bodies and extracellular infectious elementary bodies. A conserved bacterial protease, HtrA, was shown previously to be essential for *Chlamydia* during the reticulate body phase, using a novel inhibitor (JO146). In this study, isolates selected for survival of JO146 treatment were found to have polymorphisms in the acyl-acyl carrier protein synthetase gene *(aasC). AasC* encodes the enzyme responsible for activating fatty acids from host cell or synthesis to be incorporated into lipid bilayers. The isolates had distinct lipidomes with varied fatty acid compositions. A reduction in the lipid compositions that HtrA prefers to bind to was detected, yet HtrA and MOMP (a key outer membrane protein) were present at higher levels in the variants. Reduced progeny production and an earlier cellular exit were observed. Transcriptome analysis identified multiple genes were downregulated in the variants especially stress and DNA processing factors. Here we have shown that the fatty acid composition of chlamydial lipids, HtrA, and membrane proteins interplay and when disrupted impact chlamydial stress response that could trigger early cellular exit.

Introduction

Chlamydia (C.) trachomatis is a Gram-negative obligate intracellular bacterial pathogen and is a prevalent sexually transmitted infection. Infections can result in serious sequelae including pelvic inflammatory disease, tubal factor infertility, and ectopic pregnancies in women (1). All *Chlamydia spp.* have a biphasic developmental cycle with an extracellular infectious phase (elementary body, EB) and an intracellular replicative phase (reticulate body, RB) that is located inside a vacuole called the inclusion vacuole (2). As it has co-evolved with its host, *Chlamydia spp.* have undergone reductive evolution and considerable

gene loss (3). Nonetheless, *C. trachomatis* has a near complete set of genes required for phospholipid synthesis (3, 4). *C. trachomatis* can synthesise the glycerophospholipids commonly found in Gram-negative bacterial membranes including phosphatidylethanolamine (PE), phosphatidylglycerol (PG), and cardiolipin (CL). However, it relies on the host to obtain the required precursors isoleucine, serine, and glucose (5). *C. trachomatis* can only synthesise saturated, but not unsaturated, fatty acids *de novo* (3, 4, 6). The PE phospholipid class and branched chain 15:0 fatty acid species are the most abundant *C. trachomatis* lipid species (4, 7). To incorporate unsaturated fatty acids and perhaps preserve resources, *Chlamydia* activates host cell derived fatty acids using an acyl-acyl carrier protein synthetase (AasC). These activated fatty acids then enter the *de novo* biosynthetic pathways, or type II fatty acid synthesis pathway for elongation (3, 4, 6).

A chemical biology approach using an inhibitor, JO146, identified the protein HtrA to be essential for survival of *C. trachomatis* during the mid-replicative phase (8, 9). *C. trachomatis* HtrA is hypothesised to have a role in outer membrane protein stability, like its *Escherichia* (*E.*) *coli* orthologue DegP (10-12). Whilst genetic manipulation strategies have advanced (reviewed (13)) and it is now possible to implement most genetic approaches against chlamydia, high-throughput genetic methods remain limited. Hence, we implemented a random mutation and selection protocol, to further characterise the function of HtrA in *Chlamydia*. We hypothesised that mutants with resistance to the HtrA inhibitor, JO146, would identify factors that are functionally involved in HtrA's essential role for the chlamydial replicative phase. We report the selection and characterisation of three independently isolated genetic variants of *C. trachomatis* with reduced susceptibility to the previously described HtrA inhibitor JO146 (8), all three isolates had single nucleotide variants (SNVs) in *aasC* (*ct_776*). The variants had an impacted fatty acid composition, validating that the SNVs impact on function. Considerable phenotypic impacts were observed

in the isolates along with transcriptional changes, implicating a stress responses process that is likely linked to the early exit phenotype observed..

RESULTS

Chlamydial isolates with reduced susceptibility to the HtrA inhibitor JO146 all have single nucleotide variants in loci related to fatty acids

A selection experiment was conducted using repeated passage of EMS mutated and non-mutated pools of chlamydia in the presence of JO146. The purpose was to select for *C. trachomatis* isolates with resistance or reduced susceptibility to JO146 (see the Supplementary results for full details). Sequence analysis of the pools of isolates that survived the selection conditions identified four genetic hotspots that were selected for through the experiment (Supplementary Materials Table S1; CT776 (*aasC*), CT206 (putative esterase), CT544 (*uhpC*), and CT587 (enolase)). Three isolates, subsequently referred to as 1A3, 2A3, and 1B3, were cultured from independent selection pools, plaque purified (Fig. S1) and tested to confirm reduced susceptibility to JO146 (Figure 1A). 1A3 was the most susceptible isolate with similar infectious yields to wild-type (WT). 1B3 was less susceptible to JO146 than 1A3, while 2A3 was the least susceptible isolate. The isolates were characterised by whole genome sequencing, identifying that all three isolates had a distinct single nucleotide variation (SNV) in CT776, the gene encoding for *aasC* (Supplementary materials Table S2). In the case of isolate 1B3 this was the only genetic variation detected on the entire genome of the isolate characterised, meaning CT776 is solely responsible for any changes observed. In the case of 1A3 one other variation a G to A transition in a non-coding region was detected which may indicate that the CT776 change is the only functionally relevant change. There were a number of mutations in 2A3 that may be relevant to the

phenotype including in a putative esterase CT206 that was a hotspot for selection in the overall experiment (see Supplementary Table S2). CT776 is the only common gene with a SNV in all purified isolates with reduced susceptibility to JO146, and the only/major change in two of the isolates. *In silico* bioinformatics and structural modelling of the sequence variants indicated a likely impact on AasC function with all three SNV located around what appears to be a pocket in the predicted structure with impacts on hydrogen bonding (Fig. S2).

In order to assess if the loci were isolated as an indirect impact related to JO146 and HtrA function rather than being a direct 'off-target' protein that is bound by JO146 we first investigated if JO146 binds to either of the two main loci identified. We were not able to detect any evidence of binding of JO146 to either AasC or CT206. This was ruled out by AasC enzyme activity that showed no change with JO146 was added (Fig. S3). CT206 was analysed as it was initially identified in the selection pools associated with the variant 1B3 and is confirmed to be mutated in 2A3. CT206 did not bind to JO146 (cy5) using recombinant purified protein (Fig. S3), full methods outlined in the Supplementary information.

Variants have differences in infectivity, inclusion size, progeny production, and exit time frames

In order to determine what the impact of the variants or mutations have on chlamydia a series of characterisations were conducted. Phenotypic analysis was conducted on cultures in McCoy B cells in comparison to the wild-type strain (referred to as CtDpp, or WT), with infectious yield, chromosome counts, infectivity, and inclusion size assessed. This experiment was conducted in McCoy B cells as *C. trachomatis* has been observed to produce uniformly distributed growth in McCoy B cells versus patchy growth in epithelial cell lines

131 (14). The variant 1B3 had significant reductions compared to WT in inclusion forming unit
132 (IFU) production, DNA copy number, infectivity, and inclusion size (Fig. 1). Variant 1A3
133 also had reduced productivity, inclusion size, and infectivity compared to WT, although not
134 to the same extent as observed for 1B3. A live microscopy experiment was used to assess
135 chlamydial exit from the host cell, accounting for both inclusion vacuole extrusion and/or cell
136 lysis. WT and 1A3 isolates had the same range and mean time of EB release (Fig. 1). EBs
137 from both 1B3 and 2A3 variants were released earlier than both WT and 1A3 isolates (p-
138 value <0.0001; mean time of EB release: WT = 74.0 hours post infection (h PI); 1A3 = 74.6 h
139 PI; 1B3 = 65.9 h PI; 2A3 = 67.6 h PI). The overall range of EB release was smallest (more
140 synchronous and early) for the 1B3 variant, with all detected inclusion vacuoles completing
141 lysis or extrusion by 80 h PI. Examination of the gross morphology of the chlamydial
142 inclusion vacuoles, using confocal microscopy, throughout the culture phases revealed no
143 apparent differences between the variants and WT (Fig. 2).

144

145

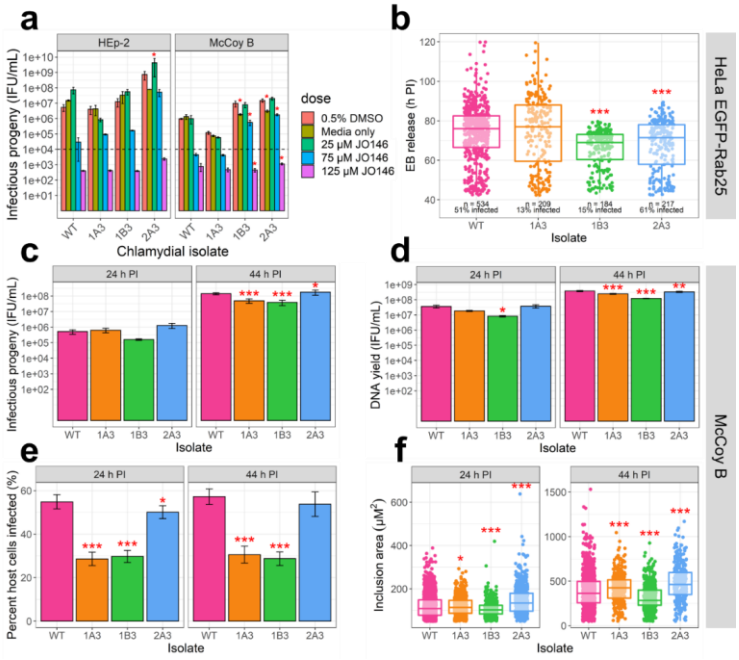

Fig. 1. Analysis of phenotypes of variants isolated with reduced susceptibility to JO146. **A.** Recovery of infectious progeny following JO146 treatment of chlamydial variants cultured in HEp-2 and McCoy B cell line that were treated at 16 h PI with JO146 doses, harvested at 44 h PI, prior to re-infection to determine IFU/ml yields indicated in this figure. Error bars represent the standard error of the mean (SEM) of three independent experiments (n=3). Dashed line indicates the threshold of accuracy ($1x10^4$ IFU/mL) for this enumeration method. *p<0.05 compared to DMSO control as measured by two-way ANOVA with Dunnett's multiple comparisons test. The % reductions for each isolate at 75 µM JO146 treatment relative to solvent are: HEp-2: 99.46%, 1A3: 97.73%, 1B3: 98.68%, 2A3: 92.87%, and McCoy B: WT: 99.53%, 1A3: 94.39%, 1B3: 94.23%, 2A3: 88.31%. **B.** EB release from cells for each isolate. Real-time microscopy analysis of EB release from HeLa EGFP-Rab25 host cells is show in hours post infection (h PI) (y axis), variants (x axis). The number of inclusions monitored and

% infectivity is indicated under the dataset for each variant. The microscopy was conducted from 42 h PI to 120 h PI with data collected every 30 mins, every visible inclusion in each field of view was monitored until no longer visible in the cell, or the cell was also no longer visible and this was recorded as the exit point. **C.** Infectious progeny yields of isolates at 24 h PI and 44 h PI. Three biological replicates were enumerated in duplicate for each isolate at each timepoint. **D.** Yield of chromosomal DNA at 24 h PI and 44 h PI, determined by qPCR. Three biological replicates were quantified in duplicate for each isolate at each timepoint. **E.** The percent of McCoy B host cells infected by each isolate at 24 h PI and 44 h PI. **F.** Inclusion vacuole size at 24 h PI and 44 h PI. Inclusion vacuole size was measured as two-dimensional area (μM^2). Triplicates of each isolate at each timepoint were visualised by microscopy with multiple fields of view or samples analysed. Error bars represent SEM from multiple experiments. *p-value $\leq$0.05, **p-value $\leq$0.001, ***p-value $\leq$0.0001, as measured by Student's t-test with Holm-Sidak's test for multiple comparisons.

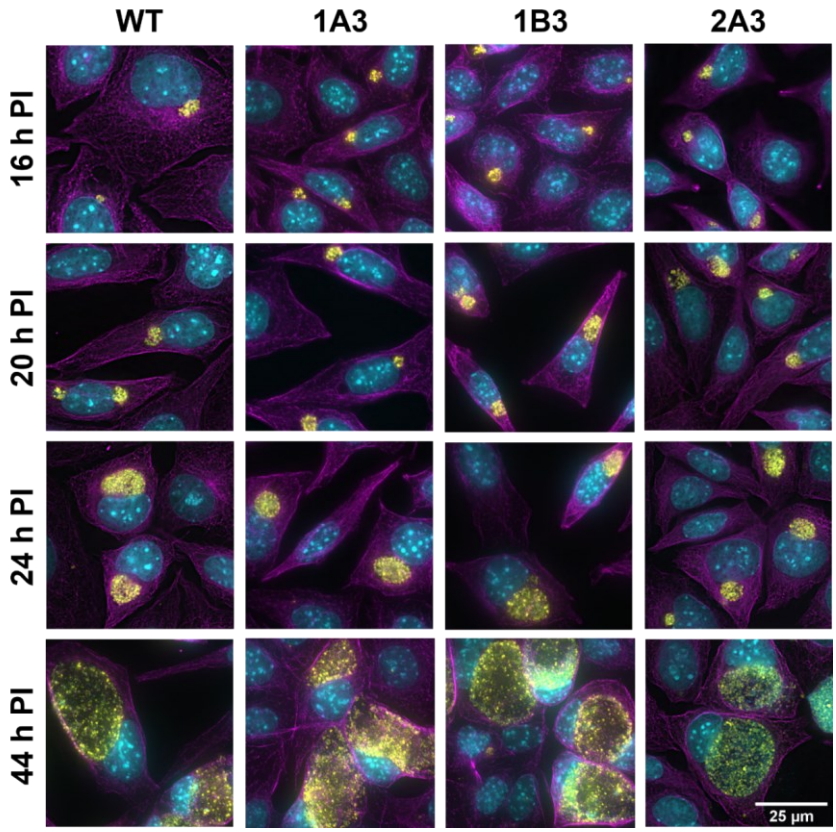

Fig. 2. Gross morphology of WT and variant chlamydial isolates at various developmental cycle phases. Cell cultures were fixed at 16, 20, 24 and 44 h PI, representing timepoints from mid-replicative phase (16 h PI) to end-replicative phase (24 h PI) and the end of EB reversion and the developmental cycle (44 h PI). Cyan = DNA, stained by DAPI; magenta = host cell cytoskeleton, specifically α-tubulin; yellow = chlamydial HtrA. Scale bar in bottom right denotes 25 µM for all panels.

Variants have distinct lipid compositions throughout the developmental cycle

We conducted a lipidomic analysis at 24 h PI and 44 h PI as the dominant role for fatty acids in bacterial cells is as constituents of the lipid bi-layer. PE and PG lipid classes were analysed as they are the major glycerophospholipid classes autonomously synthesised by *C. trachomatis* (5). A total of 116 lipids, including 75 PE species and 41 PG species were detected with robust reproducibility. In some cases in the analysis used here more than one lipid (typically isomers) were detected at the same point in the chromatogram in the workflow used for this analysis, in order to ensure accuracy of assignments or provide clarity when the assignment is ambiguous dual assignment is listed in the figure/table. A comparison of WT samples and uninfected HEp-2 cells was initially performed to select for lipids significantly increased in abundance during infection. HEp-2 cells were used as the overall yields for all variants were greater in this cell line. As the WT samples (but not variant samples) were matched with uninfected host cells as controls, exclusion of lipids not significantly associated with WT infection ensured that any significant differences between WT and variants were attributed to the bacteria. Prior to proceeding, it was confirmed that all the lipid species identified in the variants were also detected in the WT. A total of 30 lipid species, 21 PE and 9 PG, were significantly associated with *C. trachomatis* infection (Fig. 3). Of the 30 lipids associated with *C. trachomatis* infection, 24 contain the 15:0 fatty acid which is known to be abundant in *C. trachomatis* (4). A range of unsaturated fatty acids were identified to be significantly associated with infection (Table S3).

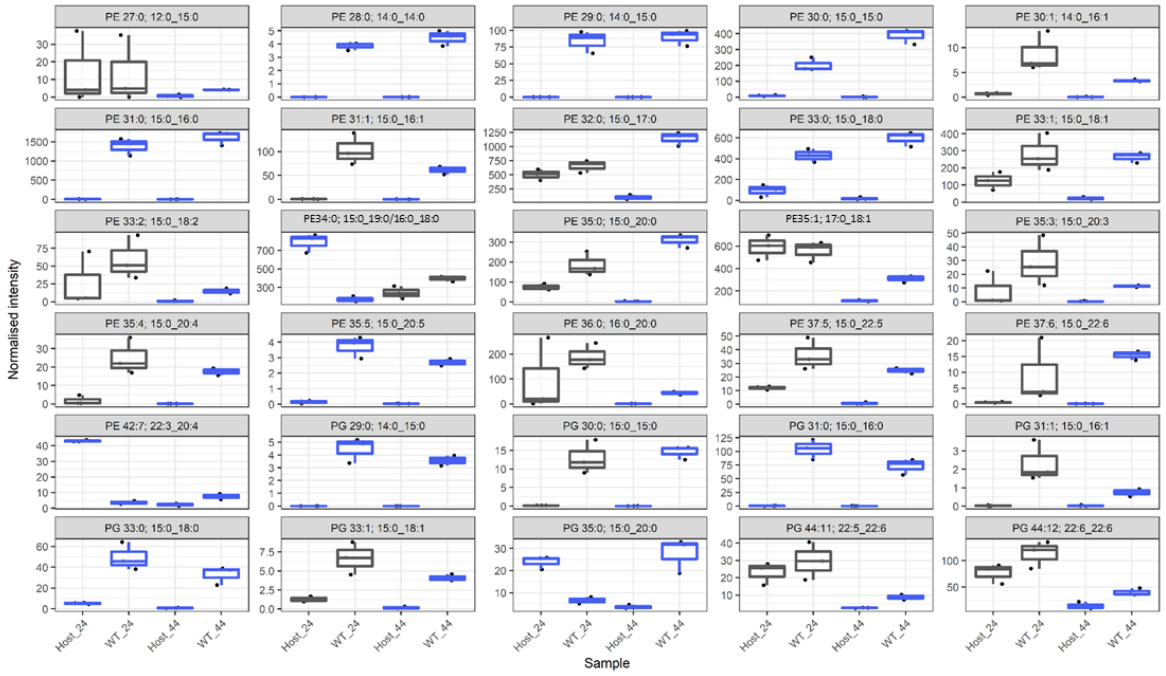

Fig. 3. Normalised intensity of 30 lipid species with significantly different abundance in WT relative to uninfected host cells. This figure identifies the lipids that are significantly associated with infection. In order to focus further analysis of the differences in the variants and WT the subsequent analysis (Fig 4 and 5) focussed only on these lipids that are significantly associated with infection. The data are presented as box plots, with the x axis indicating the sample as indicated in the bottom row. The normalised intensity is indicated by the y axis. The y axis are

intentionally different for each box as significant differences for less abundant lipids may still be biological relevant. Grey boxes indicate no significant difference at that timepoint ($p>0.05$), and blue boxes indicate a significant difference ($p<0.05$). Significance was measured via t-test ($n=3$) performed in MetaboAnalyst v5.0 as outlined in the methods. In some cases dual assignments to the same MS2 feature occurred in different specimens, this is indicated by the multiple assignments at the top of the figure for that species, PE 34:0; 15:0_19:0/16:0_18:0, and PE 35:0; 15:0_20:0/17:0_18:0.

Across the lipids significantly associated with infection we observe a substantial difference in the lipid profile of the variants compared to the WT control, with 25 significant differences identified at 24 h PI (Fig. 4 and Fig. S4). In broad terms there was an increase in most of the significantly different PE and PG species at 24 h PI with the increasing species all contained 15:0 except for PE 36:0 (PE 18:0_18:0). For example, the most abundant PE lipids associated with *C. trachomatis* infection; PE 32:0, 35:1, 34:0, 31:0, 36:0 and 33:1, were generally elevated in the variants compared to WT and except for PE 31:0, all of these lipids were significantly elevated in either 1B3 or 1B3 and 2A3. The 1A3 variant appears to be following a similar trend although the differences fail to reach significance. The trend is similar in the PG species with three of the four most abundant species; PG 44:12, PG 44:11 and PG 35:0 showing a general increase in amongst the variants (Fig. S4). A summary of the lipidomic data, listing the infection associated PE and PG lipids with significant differences between WT and any variant at either 24 or 44 h PI is shown in Table 1.

Commented [LL1]: Highlighting to check PG 44 : 12 data

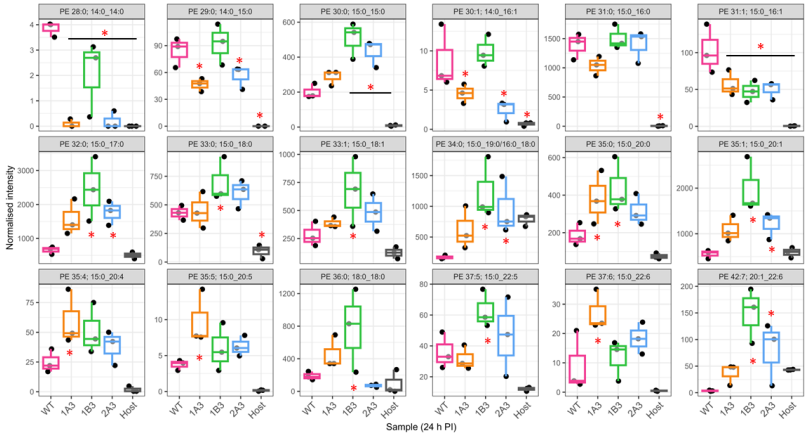

Fig. 4. Normalised intensities of PE lipid species at 24 h PI in WT, variants and host cells. The data are presented as box plots, colour coded for each strain indicated on the x axis of each box. The normalised intensities are indicated on the y axis. Different normalised intensities are used to show differences more clearly, as differences in low abundant lipids may still be biologically significant. Significance was measured by one-way ANOVA, performed using MetaboAnalyst as described in the Methods. An asterisk indicates a significant difference ($p<0.05$) in normalised intensity compared to WT (n=3 each). The best match /assignment across the samples is identified in the graphs, noting assignments can vary based on the methodology used. In some cases, more than one best match /assignment from the MS/ MS data is potential both are listed in the figure (e. g. PE34:0 15:0_19:0/16:0_18:0).

In contrast to the general increased trend amongst the infection associated PE and PG species, PE 28:0, 29:0, 30:1 and 31:1 as well as PG 29:0 and 31:1 all showed evidence of a decrease relatively to WT. These lipids comprise all of the lipids associated with infection which contain 14:0 and with the exception of PE/PG 31:1 they all contain this fatty acid. Similarly, PE/PG 31:1 and PE 30:1 was all decreased and comprise the set of 16:1 containing lipids examined here. Taken together this suggests an underlying decrease in 14:0 and 16:1 incorporation in the bacterial membrane is associated with a reduced susceptibility to JO146.

Analysis of lipid intensities 44 h PI demonstrated significant differences between strains (adjusted $p<0.05$) in 17 lipids, with 13 determined to be non-significant (Fig. 5 and Fig. S5). PE 28:0 (14:0_14:0) was significantly lower in abundance in the variants compared to WT result (as at 24 h PI) (Fig. S5). PE 29:0 (14:0_15:0) was lower in abundance at 24 h PI in 1A3 and 2A3 and by 44 h PI, this lipid was also significantly decreased in 1B3. Conversely, to 24 h PI, no significant differences in PE 30:0 (15:0_15:0) were observed between isolates. However, PE 31:0 (15:0_16:0) was found to be significantly decreased in variants compared to WT, although no differences were seen at 24 h PI. There was significantly less PE 33:0 (15:0_18:0) and PE 37:5 (15:0_22:5) in all variants compared to WT. PE 32:0 (15:0_17:0) was increased in 1B3 and 2A3 at 24 h PI but was found to be significantly increased in all three variants at 44 h PI. It was the only lipid found to have an increased abundance in variants compared to WT at this timepoint. One PG species had a significantly smaller normalised intensity in all three variants compared to WT, PG 33:0 (15:0_18:0). 1A3 had significantly less PG 29:0 (14:0_15:0), which was also observed at 24 h PI. 1A3 and 1B3 had significantly less PG 33:1 (15:0_18:1) than WT, with large variation in this lipid for 2A3.

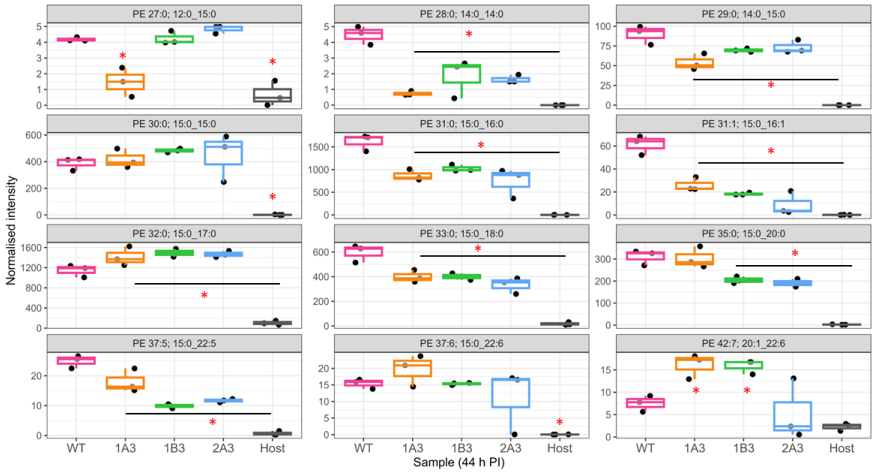

Fig. 5. Normalised intensities of PE lipids at 44 h PI in WT, variants, and host cells. The data are presented as box plots, colour coded for each strain indicated on the x axis of each box. The normalised intensities are indicated on the y axis. Different normalised intensities are used to more clearly show differences, as differences in low abundant lipids may still be biologically significant. Significance was measured by one-way ANOVA, performed using MetaboAnalyst as described in the methods. Each species is indicated in the grey bar at the top, WT, variants and host cell only is indicated on the x axis. An asterisk indicates a significant difference ($p<0.05$) in normalised intensity compared to WT (n=3 each). The best match /assignment across the samples is identified in the graph.

Changes in lipid composition changes do not affect cellular access for JO146 but likely impact the HtrA-membrane interaction, and the protein composition of the membranes

The reduced susceptibility to JO146 observed could be a consequence of reduced cellular access of JO146 mediated by the distinct lipid compositions of the variants. A JO146 – JO146-Cy5 cell permeability and competitive binding assay was performed at the replicative phase of growth to assess cellular access. Cultures were treated with JO146 (an irreversible binding mechanism) and then competitive binding of JO146Cy5 on lysates subsequently conducted to determine if there was differences in access to the JO146 relative to total HtrA levels. There was no significant difference in JO146 access and binding detected once the normalised levels of HtrA were analysed (Fig. 6). These data, whilst semi-quantitative, suggest that the reduced susceptibility to JO146 does not relate to reduced cellular access of the compound.

The connection between HtrA inhibition (via the JO146 selection) and changes in the lipid composition identified here led us to test for a direct HtrA interaction with lipid bilayersTethered bilayer lipid membranes (tBLMs) in conjunction with electrical impedance spectroscopy wasused to monitor changes in membrane conductance and capacitance that would only occur if a protein is binding to the membrane(15) (16). Changes in *membrane conduction* are due to a membrane disruption event altering the transport of ions in solution across the membrane. Increases in *membrane capacitances* are an indication of a decrease membrane thickness and/or the presence of water in the membrane. Recombinant HtrA was shown to cause an increase in both membrane conductance and capacitance in tBLMs; more favourablywithnegatively charged POPG (phosphatidylglycerol head group – red lines) containing tBLMs than zwitterionic POPE compositions (phosphatidylethanolamine head group – black lines) (Fig. 7). This data indicates that, inside the cells, HtrA could be closely associated with the membrane.

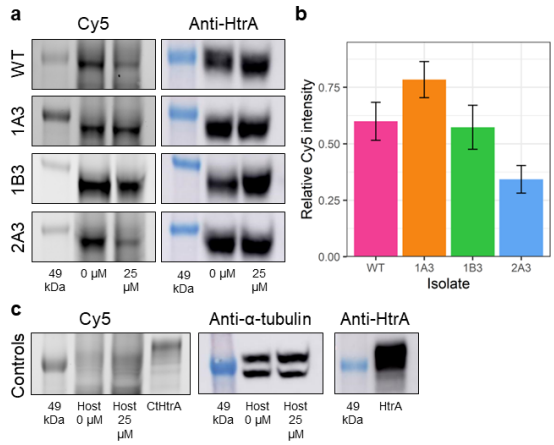

Fig. 6. SDS-PAGE gels and Western Blots of WT and mutant chlamydial lysates pre-incubated with JO146 and competitive binding with JO146-Cy5. RBs from each isolate were pre-incubated with 0 µM or 25 µM JO146. Cultures were lysed and subsequently incubated with Cy5-JO146 in a competitive binding assay to indicate permeability to JO146 of the RB or replicative phase of the cultures (consistent with the most impactful time of JO146 treatment). **A.** Representative SDS-PAGE gels (Cy-5 gel) and Western Blots (Anti-HtrA) for each chlamydial isolate, with the 49 kDa molecular weight marker indicated in the left most lane of each image. **B.** Signal intensity of Cy5 following incubation with 25 µM JO146, relative to 0 µM, and normalised to the relative intensity of anti-HtrA, as described in the supplementary methods section. **C.** Representative SDS-PAGE gels and Western Blots for host-only uninfected controls and recombinant HtrA. These are controls to demonstrate gel loading consistency. Error bars represent the SEM (n=3). Statistical differences in the normalised intensity of Cy5 in cells pre-incubated with 25 µM relative to the untreated controls was tested using one way ANOVA. There was no significant difference between WT and any mutant.

To determine if the changed lipid profile impact on the abundance of key proteins western blot analysis was conducted on selected protein targets on 44 h PI cultures. HtrA and the membrane proteins MOMP and PmpD were found to be higher in protein abundance in the variants than WT (Fig. 7). HtrA and MOMP intensities were measured using densiotometry and both were significantly higher than in WT (1.7-2.2x and1.5-1.8x higher respectively). In order to determine if this was mediated by transcriptional changes we conducted RT-qPCR analysis of these targets, *aasC*, and developmental stage genes. Transcript levels for almost all genes measured demonstrated no significant changes, with $\log_2$FC of <1 between WT and variants at 24 and 44 h PI (Fig. S6). Transcripts measured included *aasC* (*CT776*), *htrA*, *hsp60* which, like *htrA*, is involved in the stress response; *euo*, a transcriptional repressor; and two genes encoding outer membrane proteins, *omcB* and *ompA (momp)* were assessed with *16S rRNA* as the normalising gene, and *rpoB* (an additional housekeeping gene). In 1B3 at 24 h PI, *hsp60* was 1.3-fold down-regulated (p-value <0.05); however, this result was not replicated at 44 h PI or in any other isolate (Figure S6). The localisation of chlamydial proteins (HtrA, MOMP, Hsp60, RpoB) in WT and variants was assessed by confocal microscopy at 44 h PI in HEp-2 cell cultures and revealed no detectable differences in protein localisation between any isolates at this resolution (Fig. 8).

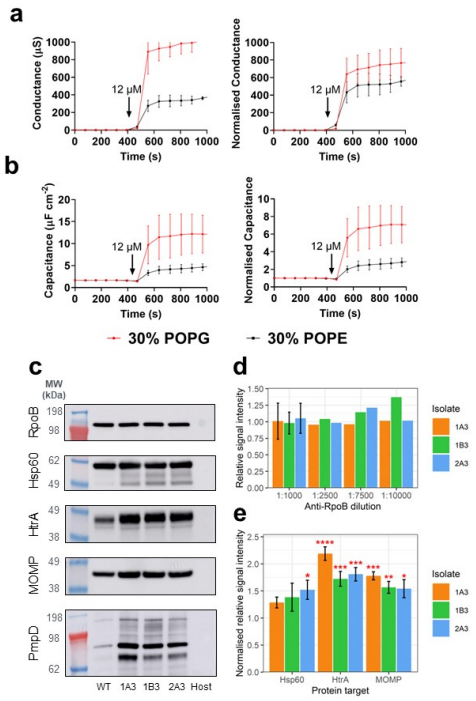

354

355 **Fig. 7. Chlamydial HtrA binding to tethered lipid bi-layer, and chlamydial protein levels.**
356 The figure shows the **A.** membrane conductance and **B.** capacitance changes (a measure of
357 membrane thickness and/or water content) to lipid bi-layers after addition of HtrA**.** The data is
358 membrane conductance (top, y-axis), and capacitance (bottom, y-axis) with the two distinct
359 membrane compositions tested (red line 30% POPG, black line 30% POPE). The arrow indicates
360 the time point that recombinant protein was added. **C.** Representative images of each Western
361 Blot. Host = uninfected host-only control**.** Western Blots of select stress response and membrane
362 proteins in WT and variant chlamydial lysates**.** EBs from each isolate were harvested at 44 h PI
363 from cultures infected with standardised MOIs, and Western Blots were performed to assess
364 relative quantities of the proteins RpoB, Hsp60, HtrA, MOMP, and PmpD. **D.** Signal intensity
365 of RpoB across a dilution series, relative to WT. **E.** Relative signal intensity of Hsp60, HtrA and

366 MOMP in each mutant, normalised to the mean RpoB relative intensity (PmpD was not analysed
367 due to the multiple bands). Error bars represent the SEM (n=3). *p<0.05; **p<0.01; ***p<0.001;
368 ****p<0.0001 compared to RpoB as measured by two-way ANOVA with Dunnett's multiple
369 comparisons test.

370

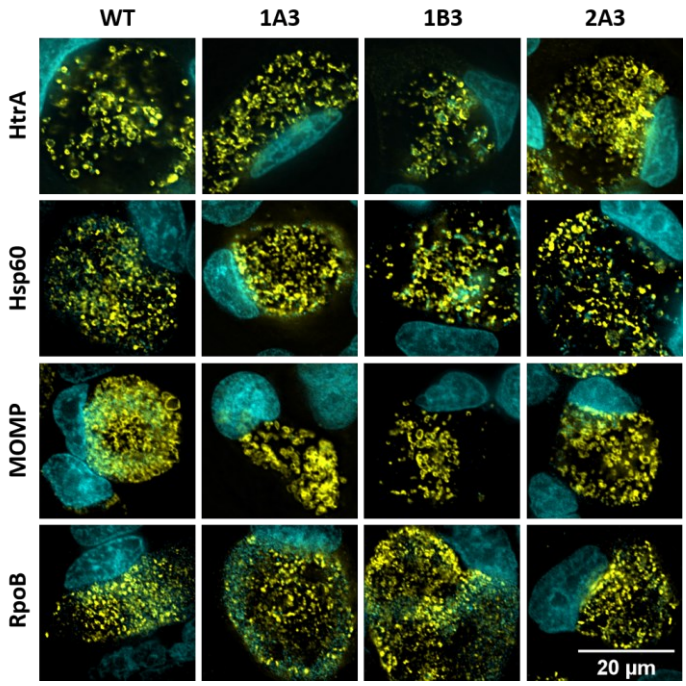

371

372 **Figure 8. Protein localisation in WT and variants.** Infected cell cultures were fixed to slides
373 and HtrA, Hsp60, MOMP and RpoB proteins were immunocytochemically labelled, visible in
374 yellow. Mammalian and bacterial DNA were labelled with DAPI, visible in cyan. Scale bar
375 denotes 20 µM for all panels.

Variants have altered gene expression profiles for early and mid-developmental cycle genes

Given the changes in some protein abundance, and HSP60 transcript change detected at 24 h PI we considered that there may be other genes with distinct expression profiles in the variants. RNA-sequencing was conducted at 20, 36, and 44 h and the transcriptome of the variants was compared to the WT (Supplementary Materials Table S5). In all variants compared to WT 46, 5 and 7 genes were significantly downregulated at 20, 36 and 44 h, respectively (fold change <2, p-adjust <0.05) (Table 2). No upregulated genes were common in all variants compared to WT. CT158, a putative phospholipase gene was significantly downregulated at 36 and 44 h PI. DNA processing related genes, genes encoding virulence proteins, protein fate factors, and some developmental cycle phasing factors, were impacted (including some Inc proteins and Tsp at 20 h PI).

DISCUSSION

In this study, selection of *C. trachomatis* variants with resistance to JO146, an inhibitor of HtrA, resulted in three isolates carrying SNVs in the *aasC* gene, encoding the acyl-acyl carrier protein synthetase. AasC is the enzyme responsible for activating and ligating fatty acids scavenged from the host for incorporation into phospholipids (5). The variants had distinct PE and PG lipid species when compared to the wild-type. Notably there was a substantial increase in PE species containing the 15:0 fatty acid and a decrease in PE and PG species containing either a 14:0 or 16:1 fatty acid in the JO146 resistant variants compared to WT. These results

suggest that the variants may increase *do novo* fatty acid synthesis of which 15:0 while concurrently reducing incorporation of myristic (14:0) and palmitoleic (16:1) fatty acid derived from the host cell. CT158, a phospholipase gene which has previously been reported as likely involved in hydrolysing host phosphatidylcholine for lipid update (17) was also significantly downregulated in gene expression at later stages of the developmental cycle for the variants, as were stress response and DNA processing factors. The variants had an increase in the abundance of HtrA and MOMP proteins, not mediated by transcription. The increased levels of these proteins are likely due to the variation in the physicochemical or biophysical properties of the membrane bilayer impacting protein interactions and stability. Recombinant HtrA showed a lower binding preference for lipids with a PE group compared to PG, which could indicate that HtrA may have less contact with the membrane in the variants which have higher PE abundance. Despite differences in the lipid profiles, the variants were not significantly less permeable to JO146 than WT. The isolate (1B3) with the most notable of these phenotypic differences, including reduced infectivity, reduced progeny production, earlier exit, also had the most marked shifts in PE and PG lipid compositions.

Given the asynchronous nature of chlamydial growth it is important to validate that the selection protocol is valid. As the selection experiment resulted in consistent selection of distinct variants in *aasC* in the three isolates characterised, this support a stringent selection. All were associated with reduced susceptibility to JO146. A range of phenotypic changes were apparent in the variants, notably a marked earlier exit and synchronicity in EB exit was apparent in two isolates, also reduced inclusion size and reduced infectious progeny, and transcriptional differences with stress response and lipid associated genes.

421 The consistent selection of SNVs in AasC led us to investigate the functional outcomes of the
422 loci being impacted using a lipidomics approach. The untargeted LC-MS/MS lipidomics
423 analysis identified all PE and PG species previously reported for *Chlamydia* validating our
424 findings are consistent with previous literature (5, 7, 18). The *aasC* variants had distinct lipid
425 profiles compared to WT, indicating that the SNVs are impacting AasC selectivity. Several
426 polyunsaturated species were increased in the variants but represented a relatively low overall
427 constituent, whilst several abundant PE species had higher abundance in the variants which
428 could indicate a shift to increased overall PE composition of the membranes. These results
429 indicate that the *aasC* variants have changed selectivity for fatty acids and that the variants are
430 increasing PE species in general. The predicted structure suggests that the site of the mutations
431 are all around a potential pocket that might be a substrate binding site. It is possible that the
432 lipids which were observed to be significantly different between WT and variants at 24 h PI but
433 not 44 h PI may reflect differences in RB vs. EB numbers rather than differences in the lipid
434 composition of RBs. For example, PE 30:0 (15:0_15:0) was significantly different in 1B3 and
435 2A3 compared to WT at 24 h PI but not at 44 h PI, owing to an increase in abundance in WT
436 ($log_2FC=0.9$, $p=0.05$) and no change in the variants at 44 h PI. Thus, for this lipid, 1B3 and
437 2A3 already had a composition at 24 h PI that was consistent with the composition of all
438 isolates at 44 h PI. The phenotypic data also indicated that 1B3 and 2A3 had a more
439 'synchronous' or earlier overall release of EBs (several other growth parameters were impacted
440 in 1B3).

441 There was also an increase in HtrA and MOMP protein abundance (in the absence of increased
442 gene transcripts). However, the mechanism of JO146 resistance in these isolates cannot be
443 explained entirely by the increase in HtrA protein, as the isolate most sensitive to JO146 (1A3)
444 also produced the most HtrA. MOMP, PmpD, and other outer membrane proteins, are
445 predicted substrates of HtrA (10-12). As HtrA was significantly increased in the variants, if the

446 increased MOMP is owing to an accumulation of unfolded protein, then this should be readily
447 degraded and cleared by HtrA. Membrane lipid composition is known to affect membrane
448 protein function and stability (reviewed, (19)), thus the variants may accommodate more
449 MOMP (and possibly other proteins) in their membranes, or the proteins are more stable and
450 accumulate over time to a greater extent. Although, HtrA was found to have reduced
451 preference for lipid bilayers with more PE headgroups, likely implicating reduced association
452 of HtrA with the membranes inside these variant cells. The differences in the transcriptome,
453 suggests an impact on the gene expression of the variants, with a variety of DNA processing,
454 stress response, and virulence factors (e.g. Inc proteins) impacted from 20-28 h PI in all three
455 variants.

456 This work demonstrates an interplay between HtrA, fatty acid metabolism, and membrane
457 proteins in *C. trachomatis*. Similar biological interactions were previously reported in *E. coli*,
458 therefore, we suggest this may be a conserved mechanism found in many bacteria. Certainly, a
459 link to stress response is well understood for many bacterial HtrA. However, the link via
460 membrane compositions is less established, the evidence for this includes; DegP (HtrA in *E.*
461 *coli*), is upregulated by a lack of cellular PE and PG (20), increased lipoproteins (21), and
462 accumulation of unfolded membrane proteins (22). DegP likely interacts with the inner
463 membrane (23, 24), and forms multimeric structures on liposomes, depending on liposome
464 fluidity (25). The phenotype and impacts here are also consistent with recent chlamydial work
465 demonstrating that developmental cycle phases, such as the RB-EB transition is based on an
466 intrinsic signal (26).

467 In summary, the continued JO146 selection over serial passages has resulted in selection for
468 variants with altered phospholipid composition, increased levels of HtrA and outer membrane
469 proteins, and several phenotypic impacts including earlier cellular exit and less infectious
470 progeny production in the most impacted variant. This implies that HtrA and membrane

protein-lipid compositions are part of chlamydial stress response which may impact cellular exit.

MATERIALS AND METHODS

Chlamydia culture and phenotypic assays

HEp2 (human epithelial type 2, ATCC® CCL-23™) were used in most cell culture experiments and for all maintenance cultures and bulk growth. *Chlamydia trachomatis* D/UW-3/Cx (ATCC VR-885) was plaque-purified and this isolate (CtDpp, referred to as WT) was used to generate the variants isolated during this study. Cell cultures were routinely conducted in a 96-well plate at a density of 25,000 cells/well. *Chlamydia* cultures were conducted after 24 hours of fresh cell culture, when *Chlamydia* were added to the cultures at the stated multiplicity of infection (MOI). The infection was routinely synchronised by centrifugation at 500 ×g/28°C for 30 minutes, and at 4 h PI infectious media was replaced with fresh supplemented media (where bulking or conducting growth curves 1 µg/mL cycloheximide was added at this point). At 16 h PI cells were treated with 25 µM, 75 µM, and 125 µM doses of JO146 in addition to media only (0 µM JO146) and 0.5% DMSO controls, and impacts measured on cultures harvested at 44 h PI (or other time points as specified).

Chlamydia morphological analysis and related infectivity experiments were conducted in McCoy B (mouse fibroblasts, ATCC® CRL-1696). Human epithelial HeLa (ATCC CCL-2) cell line stably expressing EGFP-Rab25 (27) was used for the live microscopy experiment. IFU enumeration was performed as previously described (28), imaged using the IN Cell

Analyzer 2200 (Cytiva Life Sciences). Cultures were conducted with known multiplicity of infection, and in quantifications these were either normalised to achieve consistent multiplicity of infection by adding different amounts of culture, or by normalising to controls in data analysis depending on the experiment.

Generation of *C. trachomatis* variants using EMS treatment (0.2 mg/ml) and determination of the rate of mutations were performed following a previously published procedure (29, 30), outlined in detail in the Supplementary Information (in HEp-2 cells). JO146 (Boc-Val-Pro-$Val^{p}(OPh)_2$) was synthesised by Dr Joel Tyndall, the School of Pharmacy, University of Otago, New Zealand, or sourced by commercial synthesis from GL Biochem (Shanghai, China). Cy5-JO146 ([Sulfo-Cyanine5]-Val-Pro-$Val^{p}(OPh)_2$) was purchased from Cambridge Research Biochemicals, UK at >95% purity. All cell lines were confirmed every 3 months as mycoplasma free (MycoAlert™ Mycoplasma Detection Kit (Lonza, USA) as per manufacturer's instructions). C*hlamydia* DNA content was determined via qPCR targeting the *C. trachomatis tarP* gene (Applied Biosystems, USA, assay ID Ba04646249_s1), in accordance with the manufacturer's instructions.

Morphology was analysed on cell cultures that were cultured, fixed and immunolabelled essentially as previously described (using DAPI, anti-HtrA and anti-α-tubulin) (28). Cells were imaged on the DeltaVision Elite microscope (Cytiva Life Sciences). To assess infectivity and inclusion size, five FOVs were imaged per slide using the 20x lens objective. To further evaluate morphology and infectivity, one hundred FOVs per slide were imaged using the 60x oil objectives. All images were deconvolved using the softWoRx software (Cytiva Life Sciences). The percent of host cells infected and inclusion size were measured manually in Fiji (31, 32). (31, 32)

The EB release assay was conducted in the HeLa EGFP-Rab25 cells were cultured in 6-well plates at a density of 285,000 cells/well. After 24 hours, host cells were infected with *C. trachomatis* WT and isolates (1A3, 1B3 and 2A3) at a median MOI of 5. Uninfected host cells were also cultured. At 2 h PI, infectious media was removed and replaced with fresh supplemented DMEM containing 1 ug/mL cycloheximide. Live cell imaging of cultures was started at 42 h PI, near the end of the developmental cycle but before lysis begins. Prior to imaging, culture media was replaced with DMEM without phenol red (product number 21063029, Gibco, USA), and with 25 mM HEPES (4-(2-hydroxyethyl)-1-piperazineethanesulfonic acid). Cultures were imaged using the IN Cell Analyzer 2200 (Cytiva Life Sciences) with brightfield and FITC channels, at the 20x objective. Images were captured every 30 minutes, from 42 h PI to 120 h PI, and five FOVs were imaged per well. Images were analysed using Fiji software (31, 32), where EB release and percent host cells infected were manually measured. The time of EB release was counted as the timepoint at which an inclusion was no longer visible, including both lysis and extrusion. Statistical analysis was performed using GraphPad Prism 7.

Permeability assay

HEp-2 cells were cultured onto 6-well plates at a density of 300,000 cells/well. After 24 hours, host cells were infected with variants and WT at a median MOI of 18. Cells were centrifuged at 500 ×g/28°C for 30 minutes to synchronise, and media was replaced with fresh supplemented DMEM containing 1 µg/mL cycloheximide at 2 h PI. At 20 h PI, duplicates of each infection were treated with 0 µM or 25 µM JO146 (0.5% v/v DMSO). At 22 h PI, cells were washed with DMEM twice, then harvested via scraping into SPG. Cells were concentrated by centrifugation initially at 500 ×g for 5 minutes, then at 18,000 ×g/1°C for 30 minutes. Cells

were resuspended in a minimal amount of dPBS, then probe sonicated at 50% amplitude for 30 seconds to lyse host cells and RBs. Cells were treated with 12.5 µM of Cy5-JO146 and incubated at 37°C for 30 minutes to allow binding. Approximately 0.6 µg of recombinant CtHtrA was also treated with 1 µM Cy5-JO146 at 37°C for 30 minutes as a positive control. PAGE analysis of the extracts was conducted followed by imaging of the gels at 635 nm using the Typhoon FLA 9500 (Cytiva Life Sciences). Western Blots were performed as previously described (28). Densitometry analysis of Western Blots was performed with Image Studio™ Lite (LI-COR Biosciences, USA). Local background subtraction was performed, where the median intensity value of a 3 px wide perimeter around each defined sample area was subtracted from the total pixel intensity for each sample. The intensity of Cy5 following pre-incubation with 25 µM JO146 (relative to 0 µM controls) was normalised to the intensity of anti-HtrA at 25 µM relative to 0 µM controls.

Immunoblot

Pooled EBs from *C. trachomatis* culture biological quadruplicates of each isolate (WT, 1A3, 1B3 and 2A3), and an uninfected host control lysate, were prepared and anaylsed for immunoblots. Relative protein densities were measured for normalisation of sample loading. Normalised loading between isolates was first confirmed via Western Blot using RpoB as a normalising housekeeping protein, probed with anti-RpoB in a dilution series ranging from 1:1000 to 1:10,000. Western Blots were performed with other primary antibodies as follows: anti-Hsp60 diluted 1:5000; anti-HtrA diluted 1:1000; anti-MOMP diluted 1:1000; anti-PmpD diluted 1:1000. Each blot was performed in triplicate, except for PmpD, which was performed in duplicate. Densitometry analysis of Western Blots with n=3 was performed with Image Studio™ Lite (LI-COR Biosciences, USA).

Sequencing and analysis

The wild type strain (CtDpp, or referred to as WT), cultured isolates from the experiments, and the original 6 pools from the selection experiment after three rounds of outgrowth without JO146 (passage 29) were whole genome sequenced. DNA extracted with the DNeasy mini kit (Qiagen) according to manufacturer's instructions. DNA libraries were prepared using NexteraXT library preparation kit and sequenced on the Illumina MiSeq (2 x 300bp). Trimmomatic (v 0.39) and FastQC (v 0.11.9) were used to trim and assess read quality, respectively (33). After trimming, reads were mapped to the reference genome (*C. trachomatis* D/UW-3/Cx ASM872v1) using BWA mem (v 0.7.17) with default settings. Any unmapped reads were then mapped to the plasmid sequence (pCTDEC1 CP002053.1). SNV calling was performed using Bcftools mpileup (v 1.15.1) and filtered using the following criteria: base quality ≥20, number of reads supporting the SNV ≥20 and proportion of mapped reads supporting the SNV ≥70% (34). Due to the low coverage in some mutant pool samples, SNVs with <20 reads support were manually verified using IGV (v 2.15.4) to ensure the call is supported (35). For RNA-sequencing, Mccoy cells were infected with WT and variants in biological triplicates and RNA harvested at 20, 36 and 44 h post-infection using the RNeasy plus mini kit (Qiagen). Total RNA libraries were prepared using the Illumina stranded total RNA library kit with Ribo Zero plus to deplete rRNA. The libraries were then sequenced on the NovaSeq 6000 S4 2x150bp flow cell at the UNSW Ramaciotti Centre for Genomics. FastQC was used to assess read quality and then mapped to the *C. trachomatis* D/UW-3/Cx ASM872v1 reference using Salmon v1.9. DESeq2 (v1.38.3) was used to identify significantly differentially expressed genes (fold change > 2 and p-adjust <0.05).

589

590 **PCR, RT-PCR, and Sanger sequencing**

591 Primers were manually designed to produce an amplicon of the appropriate regions of the
592 genes CT206, CT390, CT664 and CT776, to evaluate the conservation of the polymorphisms
593 selected in the original screen. RT-qPCR and primers design was conducted using standard
594 methods (primer sequences and conditions are provided in the supplementary materials (36-
595 38)). The comparative Ct method (39) was used to calculate $\log_2$ fold change (FC), and a
596 $\log_2 FC \geq 1$ was set as the threshold of significance.

597

598 **Lipidomics for comparative relative lipid profiles**

599 HEp-2 cell cultures of the isolates harvested at 24 and 44 h PI were used for lipidomic analysis.
600 The amount of *Chlamydia* in each sample was normalised to an equivalent of $7x10^6$ IFU for all
601 infected samples. Host-only controls were matched to the average volume of WT used for each
602 timepoint. To account for loss and variance during sample processing, 2.5 µg of SPLASH
603 LIPIDOMIX Mass Spec Standard (Avanti Polar Lipids, USA) was added to each normalised
604 sample as an internal standard. Lipid analysis was performed online by liquid chromatography
605 tandem mass spectrometry (LC-MS/MS). Samples were injected onto a Q Exactive™ HF-X
606 Hybrid Quadrupole-Orbitrap Mass Spectrometer (Thermo Fisher Scientific, USA) using a
607 Vanquish Horizon Ultra-High Performance Liquid Chromatograph (UHPLC) system (Thermo
608 Fisher Scientific, USA) coupled to a 100 mm x 2.1 mm Accucore Vanquish C18 column
609 (Thermo Fisher Scientific, USA). Sample loading, scan conditions, and coefficient of variation
610 analysis are described in full in the supplementary materials. The obtained CV values are in
611 line with those previously reported and demonstrate good technical reproducibility (40, 41).
612 Lipids were identified by searching the MS/MS spectra of selected model samples (WT 24 h PI

replicate #2, WT 44 h PI replicate #2, and PQC replicate #1) against LipidBlast (v10 Hiroshi Tsugawa fork)(42) and modified to include the labelled SPLASH standards using MSPepSearch (National Institute of Standards and Technology, USA). Extracted ion chromatograms corresponding to these putatively identified lipids were then extracted using MZmine 2.32 (43). Assignments corresponding to PE and PG species were then manually reviewed based on their retention times relative to other species of the same lipid class. Only PE and PG species were analysed based on previous literature demonstrating these to be the main glycerophospholipid classes synthesised by *C. trachomatis* (4). The raw files were converted to mzXML files using MSConvert (44) with centroiding, which were then processed with MZmine 2.26 (43) using the targeted feature extraction module to extract ion chromatograms corresponding to the putatively identified PG and PE species, or multiple possible species (full methodological details are provided in the supplementary materials). The lipids here were annotated at molecular species level, meaning the constituent fatty acid are identified but their *sn*-position or additional details such as double bond are not (45). The ambiguity with regards to *sn*-position is reflected in the use of an underscore between fatty acids in the shorthand nomenclature. This level of annotation is possible because of the formation of product ions in negative mode PE and PG species characteristic of the constituent fatty acids but does not typically reflect their *sn*-position (46, 47). Data normalisation and missing value imputation was performed using MetaboAnalyst v5.0 (48).

AasC assay

AasC was purified as described (4). The assays contained 100 mM Tris pH 8.0, 10 mM $MgCl_2$, 1% Triton X-100, 5 mM ATP, 2 mM DTT, 100 µM *S. aureus* ACP, 150 µM [^{14}C]palmitic acid and AasC in a final volume of 50 µl. AasC was added last to start the

reaction. Reactions were incubated at 37°C for 15 minutes, then 40 µl was spotted on Whatman 3MM paper and dried to stop the reaction. The papers were washed twice for 20 minutes each in chloroform:methanol:acetic acid (3:6:1, v/v), dried and [^{14}C]acyl-ACP formation was determined using a scintillation counter. Compound J0146 was dissolved in DMSO and two-fold serial dilutions were made. The final DMSO concentration in all assays was 4%.

Fatty acid extraction and analysis

Fatty acids were extracted from Chlamydia cultures 44 h PI and was analysed as previously described using gas chromatography-mass spectrometry (GC-MS) (49), compared to an external standard (Bacterial Acid Methyl Esters; BAMEs; 47080-U, Sigma Aldrich).

Tethered bilayer lipid membranes (tBLMs) to assess HtrA binding to lipids

Tethered Bilayer Lipid Membranes (tBLMs) were prepared using a "T10" architecture consisting of 10% benzyl-disulfide (tetra-ethyleneglycol) C20-phytanyl "tethering" molecules interspersed with 90% benzyl-disulfide-tetra-ethyleneglycol-OH "spacer" molecules were analysed for lipid binding, as previously described (15). These molecules were coordinated onto 2.1 mm^2 gold tethering electrodes (*SDx Tethered Membranes Pty Ltd, Australia*) (16). Two different mobile lipid phases were investigated: either 70% 1-palmitoyl-2-oleoyl-sn-glycero-3-phosphocholine (POPC) with 30% palmitoyl-oleoyl-phosphatidylglycerol (POPG) (mol/mol); or 70% POPC with 30% 1-palmitoyl-2-oleoyl-sn-glycero-3-phosphoethanolamine (POPE) (mol/mol) (Avanti Lipids, USA). Changes in membrane conduction and capacitance

resulting from the addition of the recombinant HtrA protein (prepared as previously described (50)) were measured using AC electrical impedance spectrometry. This utilized a 50-mV peak-to-peak AC excitation spanning the frequency range of 0.1 to 2000 Hz, with four steps per decade. The measurements were recorded using a TethaPod™ electrical impedance spectrometer operated with TethaQuick™ software (*SDx Tethered Membranes Pty Ltd, Australia*).

Statistical and data analysis

All experiment data (other than lipidomics) was analysed, graphically displayed, and statistically analysed using GraphPad Prism 7 and R (v4.2.2).

Data availability

Data is available at EBA Project Accession number PRJEB12312.

ACKNOWLEDGEMENTS

The authors thank Professor Harlan Caldwell for the supply of PmpD antibody, Lazlo Kari (exchange and discussion on chlamydial genetics), Joel Tyndall for preparation and supply of JO146. The lipidomic part of this research was facilitated by access to Sydney Mass Spectrometry, a core research facility at the University of Sydney. The authors acknowledge the use of equipment and software in the Microbial Imaging Facility in the Faculty of Science at the University of Technology Sydney. NS was supported by a UTS Faculty of Science HDR Scholarship. LL was supported by a UTS Chancellor's Research Fellowship. VO was supported by a QUT HDR Tuition Fee Award and Supervisor Scholarship. This work was

supported by National Institutes of Health grant GM034496 (C.O.R.) and ALSAC, St. Jude Children's Research Hospital. The content is solely the responsibility of the authors and does not necessarily represent the official views of the National Institutes of Health.

AUTHOR CONTRIBUTIONS

N.S. contributed to the design of the study, analysis and interpretation of the data, and drafting of the manuscript. L.L. contributed to the design of the study, analysis and interpretation of the data, and drafting of the manuscript. V. O. contributed to the design of the study, analysis and interpretation of the data relating to the initial selection experiment and drafting of the manuscript. B. A. W contributed to the analysis and interpretation of the data from the genomics and drafting of the manuscript. M. J. A. P contributed to the analysis and interpretation of the data related to HtrA lipid binding and drafting of the manuscript. L. M. contributed to the analysis and interpretation of the data related to protein binding by JO146 and drafting of the manuscript. J.R.S contributed to the analysis and interpretation of the lipidomic and culture data and drafting of the manuscript. C. K. B. contributed to the analysis and interpretation of the data lipidomic and drafting of the manuscript. C. G. C. contributed to the generation and interpretation of the HtrA lipid binding data and drafting of the manuscript. G. M. contributed to the analysis and interpretation of the data related to chlamydia culture and drafting of the manuscript. R. M. contributed to the analysis and interpretation of the data related to chlamydial culture and drafting of the manuscript. C. R. contributed to the analysis and interpretation of the data related to AasC and drafting of the manuscript. P. T. contributed to the design of the study, analysis, and interpretation of the data, and drafting of the manuscript. W. M. H. contributed to the design of the study, analysis and interpretation of the data, and drafting of the manuscript.

Competing interests

The authors declare no conflicts of interest.

Supplemental material

There is additional supplemental material.

REFERENCES

1. Menon S, Timms P, Allan JA, Alexander K, Rombauts L, Horner P, Keltz M, Hocking J, Huston WM. 2015. Human and Pathogen Factors Associated with Chlamydia trachomatis-Related Infertility in Women. Clin Microbiol Rev 28:969-85.
2. Hogan R, Mathews SA, Mukhopadhyay S, Summersgill JT, Timms P. 2004. Chlamydial persistence: beyond the biphasic paradigm. Infection and Immunity 72:1843-1855.
3. Stephens RS, Kalman S, Lammel C, Fan J, Marathe R, Aravind L, Mitchell W, Olinger L, Tatusov RL, Zhao QX, Koonin EV, Davis RW. 1998. Genome sequence of an obligate intracellular pathogen of humans: Chlamydia trachomatis. Science 282:754-759.
4. Yao J, Dodson VJ, Frank MW, Rock CO. 2015. Chlamydia trachomatis Scavenges Host Fatty Acids for Phospholipid Synthesis via an Acyl-Acyl Carrier Protein Synthetase. J Biol Chem 290:22163-73.
5. Yao J, Cherian PT, Frank MW, Rock CO. 2015. Chlamydia trachomatis Relies on Autonomous Phospholipid Synthesis for Membrane Biogenesis. J Biol Chem 290:18874-88.
6. Yao J, Abdelrahman YM, Robertson RM, Cox JV, Belland RJ, White SW, Rock CO. 2014. Type II fatty acid synthesis is essential for the replication of Chlamydia trachomatis. J Biol Chem 289:22365-76.
7. Wylie JL, Hatch GM, McClarty G. 1997. Host cell phospholipids are trafficked to and then modified by *Chlamydia trachomatis*. J Bacteriol 179:7233-42.
8. Gloeckl S, Ong VA, Patel P, Tyndall JD, Timms P, Beagley KW, Allan JA, Armitage CW, Turnbull L, Whitchurch CB, Merdanovic M, Ehrmann M, Powers JC, Oleksyszyn J, Verdoes M, Bogyo M, Huston WM. 2013. Identification of a serine protease inhibitor which causes inclusion vacuole reduction and is lethal to Chlamydia trachomatis. Molecular Microbiology 89:676-89.
9. Ong VA, Marsh JW, Lawrence A, Allan JA, Timms P, Huston WM. 2013. The protease inhibitor JO146 demonstrates a critical role for CtHtrA for Chlamydia trachomatis reversion from penicillin persistence. Front Cell Infect Microbiol 3:100.
10. Huston WM, Tyndall JD, Lott WB, Stansfield SH, Timms P. 2011. Unique residues involved in activation of the multitasking protease/chaperone HtrA from Chlamydia trachomatis. PLoS One 6:e24547.

11. Marsh JW, Lott WB, Tyndall JD, Huston WM. 2013. Proteolytic activation of Chlamydia trachomatis HTRA is mediated by PDZ1 domain interactions with protease domain loops L3 and LC and beta strand beta5. Cell Mol Biol Lett doi:10.2478/s11658-013-0103-2:522-537.
12. Marsh JM, Ong VA, Lott WB, Timms P, Tyndall JDA, Huston WM. 2017. CtHtrA: the lynchpin of the chlamydial surface and a promising therapeutic target Future Microbiol 10:2217.
13. Wan W, Li D, Li D, Jiao J. 2023. Advances in genetic manipulation of *Chlamydia trachomatis*. Front Immunol 14:1209879.
14. Guseva NV, Dessus-Babus S, Moore CG, Whittimore JD, Wyrick PB. 2007. Differences in Chlamydia trachomatis serovar E growth rate in polarized endometrial and endocervical epithelial cells grown in three-dimensional culture. Infection and Immunity 75:553-64.
15. Berry T, Dutta D, Chen R, Leong A, Wang H, Donald WA, Parviz M, Cornell B, Willcox M, Kumar N, Cranfield CG. 2018. Lipid Membrane Interactions of the Cationic Antimicrobial Peptide Chimeras Melimine and Cys-Melimine. Langmuir 34:11586-11592.
16. Cranfield CG, Cornell BA, Grage SL, Duckworth P, Carne S, Ulrich AS, Martinac B. 2014. Transient potential gradients and impedance measures of tethered bilayer lipid membranes: pore-forming peptide insertion and the effect of electroporation. Biophys J 106:182-9.
17. Nelson DE, Crane DD, Taylor LD, Dorward DW, Goheen MM, Caldwell HD. 2006. Inhibition of Chlamydiae by primary alcohols correlates with the strain-specific complement of plasticity zone phospholipase D genes. Infection and Immunity 74:73-80.
18. Bidawid S, Chou S, Ng CW, Perry E, Kasatiya S. 1989. Fatty acid profiles of Chlamydia using capillary gas chromatography. Antonie Van Leeuwenhoek 55:123-32.
19. Zhang YM, Rock CO. 2008. Membrane lipid homeostasis in bacteria. Nat Rev Microbiol 6:222-33.
20. Rowlett VW, Mallampalli VKPS, Karlstaedt A, Dowhan W, Taegtmeyer H, Margolin W, Vitrac H. 2017. Impact of Membrane Phospholipid Alterations in Escherichia coli on Cellular Function and Bacterial Stress Adaptation. J Bacteriol 199:e00849-16.
21. Miyadai H, Tanaka-Masuda K, Matsuayama S, Tokuda H. 2004. Effects of lipoprotein overproduction on the induction of DegP (HtrA) involved in quality control in the *Escherichia coli* periplasm. Journal of Biological Chemistry 279:39807-39813.
22. Meltzer M, Hasenbein S, Mamant N, Merdanovic M, Poepsel S, Hauske P, Kaiser M, Huber R, Krojer T, Clausen T, Ehrmann M. 2009. Structure, function and regulation of the conserved serine proteases DegP and DegS of Escherichia coli. Res Microbiol 160:660-6.
23. Skorko-Glonek J, Lipinska B, Krzewski K, Zolese G, Bertoli E, Tanfani F. 1997. HtrA heat shock protease interacts with phospholipid membranes and undergoes conformational changes. Journal of Biological Chemistry 272:8974-8982.
24. Krojer T, Pangerl K, Kurt J, Sawa J, Stingl C, Mechtler K, Huber R, Ehrmann M, Clausen T. 2008. Interplay of PDZ and protease domain of DegP ensures efficient elimination of misfolded proteins. PNAS 105:7702.
25. Shen QT, Bai XC, Chang LF, Wu Y, Wang HW, Sui SF. 2009. Bowl-shaped oligomeric structures on membranes as DegP's new functional forms in protein quality control. PNAS 106:4858.
26. Chiarelli TJ, Grieshaber NA, Omsland A, Remien CH, Grieshaber SS. 2020. Single-Inclusion Kinetics of *Chlamydia trachomatis* development. mSystems 5:e00689-20.
27. Kerr MC, Gomez GA, Ferguson C, Tanzer MC, Murphy JM, Yap AS, Parton RG, Huston WM, Teasdale RD. 2017. Laser-mediated rupture of chlamydial inclusions triggers pathogen egress and host cell necrosis. Nat Commun 8:14729.
28. Huston WM, Theodoropoulos C, Mathews SA, Timms P. 2008. Chlamydia trachomatis responds to heat shock, penicillin induced persistence, and IFN-gamma persistence by altering levels of the extracytoplasmic stress response protease HtrA. BMC Microbiol 8:190.
29. Kari L, Goheen MM, Randall LB, Taylor LD, Carlson JH, Whitmire WM, Virok D, Rajaram K, Endresz V, McClarty G. 2011. Generation of targeted *Chlamydia trachomatis* null mutants. Proceedings of the National Academy of Sciences 108:7189.

30. Binet R, Maurelli AT. 2005. Frequency of spontaneous mutations that confer antibiotic resistance in Chlamydia spp. Antimicrob Agents Chemother 49:2865-73.
31. Schindelin J, Arganda-Carreras I, Frise E, Kaynig V, Longair M, Pietzsch T, Rueden C, Saalfeld S, Schmid B, Tinevez JY, White DJ, Hartenstein V, Eliceiri K, Tomancak P, Cardona A. Fiji: an open-source platform for biological-image analysis. Nature Methods 9:676-82.
32. Schneider CA, Rasband WS, Eliceiri K. 2012. NIH Image to ImageJ: 25 years of image analysis. Nature Methods 9:671-75.
33. Bolger AM, Lohse M, Usadel B. 2014. Trimmomatic: A flexible trimmer for Illumina Sequence Data. Bioinformatics 170.
34. Li H, Handsaker B, Wysoker A, Fennell T, Ruan J, Homer N, Marth G, Abecasis G, Durbin R, 1000 Genome Project Data PS. 2009. Aligning sequence reads, clone sequences and assembly contigs with BWA-MEM. Bioinformatics 25:2078-9.
35. Robinson JT, Thorvaldsdóttir H, Winckler W, Guttman M, Lander ES, Getz G, Mesirov JP. 2011. Integrative genomics viewer. Nat Biotechnol 29:24-26.
36. Bahshmakov Y, Zigangirova N, Pashko Y, Kapotina L, Petyaev I. 2010. *Chlamydia trachomatis* growth inhibition and restoration of LDL-receptor level in HepG2 cells treated with mevastatin. Comparative Hepatology 9:3.
37. Huston W, Lawrence A, Wee B, Thomas M, Timms P, Vodstrcil L, McNulty A, McIvor R, Worthington K, Donovan B, Phillips S, Chen M, Fairley C, Hocking J. 2022. Repeat infections with chlamydia in women may be more transcriptionally active with lower responses from some immune genes. Frontiers in Public Health 10:1012835.
38. Nunes A, Gomes JP, Mead S, Florindo C, Correia H, Borrego MJ, Dean D. 2007. Comparative expression profiling of the Chlamydia trachomatis pmp gene family for clinical and reference strains. PLoS One 2:e878.
39. Schmittgen TD, Livak KJ. 2008. Analyzing real-time PCR data by the comparative CT method. Nature Protocols 3:1101-8.
40. Drotleff B, Lämmerhofer M. 2019. Guidelines for selection of internal standard-based normalization strategies in untargeted lipidomic profiling by LC-HR-MS/MS. Analytical Chemistry 91:9836-43.
41. Katajamaa M, Orešič M. 2005. Processing methods for differential analysis of LC/MS profile data. . BMC Bioinformatics 6:179.
42. Kind T, Liu K-H, Lee DY, DeFelice B, Meissen JK, Fiehn O. 2013. LipidBlast in silico tandem mass spectrometry database for lipid identification. Nature Methods 10:755-8.
43. Pluskal T, Castillo S, Villar-Briones A, Orešič M. 2010. MZmine 2: Modular framework for processing, visualizing, and analyzing mass spectrometry-based molecular profile data. BMC Bioinformatics 395:1186.
44. Holman JD, Tabb DL, Mallick P. 2014. Employing ProteoWizard to convert raw mass spectrometry data. Current Protocols in Bioinformatics 46:13-24.
45. Liebisch G, Vizcaíno JA, Köfeler H, Trötzmüller M, Griffiths WJ, Schmitz G, Spener F, Wakelam MJO. 2013. Shorthand notation for lipid structures derived from mass spectrometry. . J Lipid Res 54:1523-1530.
46. Cao W, Cheng S, Yang J, Feng J, Zhang W, Li Z, Chen Q, Xia Y, Ouyang Z, Ma X. 2020. Large-scale lipid analysis with C=C location and sn-position isomer resolving power. Nat Commun 11:375.
47. Lee H-C, Yokomizo T. 2018. Applications of mass spectrometry-based targeted and non-targeted lipidomics. Biochemical and Biophysical Research Communications 504:576-81.
48. Pang Z, Chong J, Zhou G, de Lima Morais DA, Chang L, Barrette M, Gauthier C, Jacques PÉ, Li S, Xia J. 2021. MetaboAnalyst 5.0: narrowing the gap between raw spectra and functional insights. Nucleic Acids Res 49:W388-W396.
49. Sasser M. 1990. Identification of bacteria by gas chromatography of cellular fatty acids. MIDI technical note 101. Newark, DE: MIDI inc.

50. Huston WM, Swedberg JE, Harris JM, Walsh TP, Mathews SA, Timms P. 2007. The temperature activated HtrA protease from pathogen Chlamydia trachomatis acts as both a chaperone and protease at 37 degrees C. Febs Letters 581:3382-6.

FIGURE LEGENDS

Commented [WH2]: Update figure legends at the end

Fig. 1. Analysis of phenotypes of variants isolated with reduced susceptibility to JO146. A. Recovery of infectious progeny following JO146 treatment of chlamydial variants cultured in HEp-2 and McCoy B cell line. Error bars represent the standard error of the mean (SEM) of three independent experiments (n=3). Dashed line indicates the threshold of accuracy ($1x10^4$ IFU/mL) for this enumeration method. *$p<0.05$ compared to DMSO control as measured by two-way ANOVA with Dunnett's multiple comparisons test. **B.** EB release from cells for each isolate. Real-time microscopy analysis of EB release from HeLa EGFP-Rab25 host cells is show in hours

post infection (h PI) (y axis), variants (x axis). The number of inclusions monitored and % infectivity is indicated under the dataset for each variant. **C.** Infectious progeny yields of isolates at 24 h PI and 44 h PI. Three biological replicates were enumerated in duplicate for each isolate at each timepoint. **D.** Yield of chromosomal DNA at 24 h PI and 44 h PI, determined by qPCR. Three biological replicates were quantified in duplicate for each isolate at each timepoint. **E.** The percent of McCoy B host cells infected by each isolate at 24 h PI and 44 h PI. **F.** Inclusion vacuole size at 24 h PI and 44 h PI. Inclusion vacuole size was measured as two-dimensional area (μM^2). Triplicates of each isolate at each timepoint were visualised by microscopy with multiple fields of view or samples analysed. Error bars represent SEM from multiple experiments. *p-value ≤0.05, **p-value ≤0.001, ***p-value ≤0.0001, as measured by Student's t-test with Holm-Sidak's test for multiple comparisons.

Fig. 2. Gross morphology of WT and variant chlamydial isolates at various developmental cycle phases. Cell cultures were fixed at 16, 20, 24 and 44 h PI, representing timepoints from mid-replicative phase (16 h PI) to end-replicative phase (24 h PI) and the end of EB reversion and the developmental cycle (44 h PI). Cyan = DNA, stained by DAPI; magenta = host cell cytoskeleton, specifically α-tubulin; yellow = chlamydial HtrA. Scale bar in bottom right denotes 25 μM for all panels.

Fig. 3. Box plots indicating normalised intensity of 30 lipid species with significantly different abundance in WT relative to uninfected host cells. Grey boxes indicate no significant difference at that timepoint ($p>0.05$), and blue boxes indicate a significant difference ($p<0.05$). Significance was measured via t-test ($n=3$) performed in MetaboAnalyst v5.0 as outlined in the methods. In some cases dual assignments to the same MS2 feature

occurred in different specimens, this is indicated by the multiple assignments at the top of the figure for that species, PE 34:0; 15:0_19:0/16:0_18:0, and PE 35:0; 15:0_20:0/17:0_18:0.

Fig. 4. Normalised intensities of PE lipid species at 24 h PI in WT, variants and host cells. Data are presented as box plots. Significance was measured by one-way ANOVA, performed using MetaboAnalyst as described in the Methods. An asterisk indicates a significant difference ($p<0.05$) in normalised intensity compared to WT (n=3 each). The best match /assignment across the samples is identified in the graphs, noting assignments can vary based on the methodology used. In some cases, more than one best match /assignment from the MS/ MS data is potential both are listed in the figure (e. g. PE34:0 15:0_19:0/16:0_18:0).

Fig. 5. Normalised intensities of PE lipids at 44 h PI in WT, variants and host cells. Data are presented as box plots. Significance was measured by one-way ANOVA, performed using MetaboAnalyst as described in the methods. Each species is indicated in the grey bar at the top, WT, variants and host cell only is indicated on the x axis. An asterisk indicates a significant difference ($p<0.05$) in normalised intensity compared to WT (n=3 each). The best match /assignment across the samples is identified in the graph.

Fig. 6. SDS-PAGE gels and Western Blots of WT and mutant chlamydial lysates pre-incubated with JO146 and competitive binding with JO146-Cy5. RBs from each isolate were pre-incubated with 0 μM or 25 μM JO146. Cultures were lysed and free proteins were subsequently incubated with Cy5-JO146. **A.** Representative SDS-PAGE gels and Western Blots for each chlamydial isolate, with the 49 kDa molecular weight marker indicated. **B.** Signal intensity of Cy5 following incubation with 25 μM JO146, relative to 0 μM, and normalised to

916 the relative intensity of anti-HtrA. **C.** Representative SDS-PAGE gels and Western Blots for
917 host-only uninfected controls and recombinant HtrA. Error bars represent the SEM (n=3).

918

919 **Fig. 7. Chlamydial HtrA binding to tethered lipid bi-layer, and chlamydial proteins.** The
920 figure shows the **A.** membrane conductance and **B.** capacitance changes (a measure of membrane
921 thickness and/or water content) to lipid bi-layers after addition of HtrA**.** The data is membrane
922 conductance (top, y-axis), and capacitance (bottom, y-axis) with the two distinct membrane
923 compositions tested (red line 30% POPG, black line 30% POPE). The arrow indicates the time
924 point that recombinant protein was added. **C.** Representative images of each Western Blot. Host
925 = uninfected host-only control**.** Western Blots of select stress response and membrane proteins
926 in WT and variant chlamydial lysates**.** EBs from each isolate were harvested at 44 h PI, and
927 Western Blots were performed to assess relative quantities of the proteins RpoB, Hsp60, HtrA,
928 MOMP, and PmpD. **D.** Signal intensity of RpoB across a dilution series, relative to WT. **E.**
929 Relative signal intensity of Hsp60, HtrA and MOMP in each mutant, normalised to the mean
930 RpoB relative intensity (PmpD was not analysed due to the multiple bands). Error bars represent
931 the SEM (n=3). *p<0.05; **p<0.01; ***p<0.001; ****p<0.0001 compared to RpoB as measured
932 by two-way ANOVA with Dunnett's multiple comparisons test.

933 **Figure 8. Protein localisation in WT and variants.** Infected cell cultures were fixed to slides
934 and HtrA, Hsp60, MOMP and RpoB proteins were immunocytochemically labelled, visible in
935 yellow. Mammalian and bacterial DNA were labelled with DAPI, visible in cyan. Scale bar
936 denotes 20 µM for all panels.

937

938

Table 1: Summary of PE and PG lipids identified to have significant differences between WT and any variant at either 24 h or 44 h PI.

*Bolded values indicate $p < 0.05$ (based on one-way ANOVA), non-bolded values or empty cells indicate non-significant p-values.

Lipid species		24 h Log2 FC variant vs WT*			44 h Log2 FC variant vs WT*		
		1A3	1B3	2A3	1A3	1B3	2A3
PE	PE 28:0 (14:0_14:0)	**-5.35**	**-0.90**	**-4.26**	**-2.59**	**-1.28**	**-1.45**
	PE 29:0 (14:0_15:0)	**-0.85**	0.14	**-0.58**	**-0.74**	**-0.37**	**-0.29**
	PE 30:0 (15:0_15:0)	0.51	**1.33**	**1.09**	0.11	0.32	0.21
	PE 30:1 (14:0_16:1)	**-0.94**	0.17	**-1.82**			
	PE 31:0 (15:0_16:0)	-0.42	0.12	0.01	**-0.89**	**-0.65**	**-1.13**
	PE 31:1 (15:0_16:1)	**-0.85**	**-1.12**	**-1.04**	**-1.23**	**-1.75**	**-2.77**
	PE 32:0 (15:0_17:0)	1.26	**1.90**	**1.43**	**0.31**	**0.39**	**0.36**
	PE 33:0 (15:0_18:0)	0.05	**0.70**	0.49	**-0.58**	**-0.57**	**-0.84**
	PE 33:1 (15:0_18:1)	0.46	**1.26**	0.78			
	PE 34:0 (15:0_19:0/16:0_18:0)	1.85	**2.85**	**2.48**			
	PE 35:0 (15:0_20:0)	**1.04**	**1.23**	0.76	-0.03	**-0.60**	**-0.70**
	PE 35:1 (15:0_20:1)	0.96	**1.83**	**1.12**			
	PE 35:4 (15:0_20:4)	**1.26**	1.03	0.61			
	PE 35:5 (15:0_20:5)	**1.40**	0.68	0.75			
	PE 36:0 (18:0_18:0)	1.28	**2.04**	-1.44			
	PE 37:5 (15:0_22:5)	-0.19	**0.80**	0.37	**-0.47**	**-1.33**	**-1.09**
	PE 37:6 (15:0_22:6)	**1.56**	0.35	1.00	0.35	-0.01	-0.46
	PE 42:7 (20:1_22:6)	3.34	**5.36**	**4.46**	**1.09**	**1.07**	-0.49
PG	PG 29:0 (14:0_15:0)	**-0.98**	-0.06	-0.44	**-0.74**	-0.36	-0.66
	PG 30:0 (15:0_15:0)	0.02	0.60	**0.64**			
	PG 31:1 (15:0_16:1)	**-5.47**	**-3.36**	**-4.60**			
	PG 33:0 (15:0_18:0)				**-0.83**	**-0.79**	**-0.96**
	PG 33:1 (15:0_18:1)				**-1.28**	**-1.99**	-0.74
	PG 35:0 (15:0_20:0)	0.83	**2.26**	**0.90**			

	PG 44:11 (22:5_22:6)	1.37	**1.89**	1.06			
	PG 44:12 (22:6_22:6)	1.37	**1.89**	1.06			

	PG 44:12 (22:6_22:6)	**1.37**	**1.89**	**1.06**

Che *Bolded values indicate $p < 0.05$ (based on one-way ANOVA), non-bolded values or empty cells indicate non-significant p-values.

Commented [WH3]: Check PG 44 : 12 data

Table 2. Functional categories of genes downregulated in expression in all variants compared to wild-type

		Functional Category											
	Total # Genes downregulated in variants	**Hypothetical protein**	**Deubiquitinase**	**Amino acids and derivatives**	**Co-factors, vitamins, prosthetic groups**	**DNA Processing**	**Energy and precursor metabolites**	**Fatty acids, lipids, and isoprenoids**	**Porphyrin metabolism**	**Protein fate**	**RNA processing**	**Stress response, defence, virulence**	**Transporter/binding proteins**

20 h PI	**46**	13	1	3	2	9	1	2	2	2 [@]	2	8 [&]	1
36 h PI	**5**					1			1			3[&]	
48 h PI	**7**					4			1			2[&]	

[&] including Inc proteins and phospholipase